Surface & Coatings Technology 232 (2013) 33–40

Contents lists available at ScienceDirect

Surface & Coatings Technology

journal homepage: www.elsevier.com/locate/surfcoat

Cold sprayed aluminum based glassy coating: Synthesis, wear and corrosion properties

Debrupa Lahiri [a], Puneet K. Gill [b], Sergio Scudino [c], Cheng Zhang [a], Virendra Singh [d], Jeganathan Karthikeyan [e], Norman Munroe [b], Sudipta Seal [d], Arvind Agarwal [a,*]

[a] Plasma Forming Laboratory, Department of Mechanical and Materials Engineering, Florida International University, Miami, FL-33174, United States
[b] Department of Mechanical and Materials Engineering, Florida International University, Miami, FL-33174, United States
[c] IFW Dresden, Institut für Komplexe Materialien, D-01171 Dresden, Germany
[d] AMPAC and Nanoscience Technology Center, University of Central Florida, Orlando, FL-32816, United States
[e] ASB Industries, Inc., Barberton, OH 44203-1689, United States

ARTICLE INFO

Article history:
Received 16 October 2012
Accepted in revised form 22 April 2013
Available online 29 April 2013

Keywords:
Cold spraying
Aluminum based metallic glass
Coating
Wear resistance
Corrosion resistance

ABSTRACT

Al-based glassy coatings were synthesized using cold spraying technique to protect 6061 aluminum surface from wear and corrosion. Gas atomized $Al_{90.05}Y_{4.4}Ni_{4.3}Co_{0.9}Sc_{0.35}$ (at.%) powder was used as the starting powder. Dense (98%) coatings with a uniform thickness of ~250 μm were deposited. The coatings retained the glassy structure of the powder with few nanocrystals embedded in the amorphous matrix. Ball-on-disk wear of the coatings showed 600% improvement in the wear resistance as compared to 6061Al substrate. Potentiodynamic studies of the coatings in varying NaCl concentrations displayed 5 times better corrosion resistance than 6061 Al substrate, which was attributed to the active passivation and the chemical homogeneity of the coatings.

1. Introduction

Aluminum based bulk metallic glasses (Al-BMG) have attracted a lot of attention due to their superior mechanical properties, low density and corrosion resistance [1–10]. The strength of Al-BMG could be higher than 1200 MPa at room temperature [10]. Disordered atomic arrangement in BMG structure makes the deformation difficult as compared to ordered FCC structure in Al, which has slip planes of low critical resolved shear stress (CRSS). Glassy metallic structures are also known for their superior tribological behavior, which is closely linked to their mechanical properties. Zr and Fe based bulk metallic glasses have recorded impressive improvement in the wear resistance as compared to their crystalline counterparts [11–16]. The wear in BMGs is governed both by plastic deformation from severe shear localization and abrasive wear, the characteristic of brittle materials. An interesting study by Zenebe et al. has established improved anti-corrosive wear resistance behavior of Fe-based BMG [16]. However, Al-based metallic glasses have not been studied significantly to understand their tribological behavior. The only study on micro-scale abrasion of melt-spun Al-BMG has reported wear resistance similar to hardened alloys and an increase in wear resistance after devitrification, due to nanocrystal formation [17].

Electrochemical studies on Al-BMG have shown superior corrosion resistance as compared to pure Al [5–8,18]. Xueqing et al. have studied the corrosion resistance of the melt-spun amorphous $Al_{88}Ni_6La_6$ and $Al_{86}Ni_6La_6Cu_2$ in 0.01 M alkaline NaCl [6]. Compared to Al, the amorphous alloys had a higher corrosion potential and a lower corrosion current density. Wang et al. annealed the $Al_{88}Ni_6La_6$ ribbons at 523 K for 4 min and 673 K for 15 min to obtain samples that were partially and fully devitrified and, then measured the corrosion resistance in 0.01 M NaCl [18]. The corrosion potential was higher for amorphous alloys as compared to Al. Scully et al studied the effects of heat treatment-induced devitrification on the pitting corrosion behavior of $Al_{90}Gd_5Fe_5$ and $Al_{87}Y_{4.3}Ni_{8.7}$ alloys and concluded that pitting resistance of amorphous aluminum alloys was retained even when small Al-rich nanocrystals were present in the amorphous matrix [5]. Similar improvement in the corrosion resistance of partially crystallized alloy was obtained by Lin et al. for $(Al_{86}Ni_9La_5)_{98}Zr_2$ alloy [7]. The improvement in the corrosion resistance for amorphous structure originates from the chemically homogeneous structure which is free of defects such as grain boundaries, precipitates and segregation. It has been found that partially crystallized alloys have corrosion resistance comparable to the amorphous alloy; while full crystallization reduced the corrosion resistance [7,18]. Such behavior is attributed to the creation of new interfaces that leads to easy transport of species and a faster development of passive layer.

In spite of possessing excellent corrosion and wear resistant properties, Al-BMG alloys have rarely been synthesized as protective

* Corresponding author. Tel.: +1 305 348 1701; fax: +1 305 348 1932.
E-mail address: agarwala@fiu.edu (A. Agarwal).

0257-8972/$ – see front matter © 2013 Elsevier B.V. All rights reserved.
http://dx.doi.org/10.1016/j.surfcoat.2013.04.049

coatings on a large scale. The majority of Al-based BMGs have been prepared by melt spinning technique [19–23]. The maximum thickness of Al-based BMG is limited to 100 μm due to their relatively low glass forming ability, except recently synthesized amorphous $Al_{86}Ni_8Y_6$ alloy with 1 mm thickness [24]. Fe, Ni, Cu and Zr-based metallic amorphous/partially crystalline glassy coatings have been synthesized on a large scale by thermal spray techniques, but same is not true for Al based BMGs [25–32]. This could be largely attributed to commercial non-availability of aluminum based BMG powder and rapid crystallization during most of the coating synthesis techniques. Al-based nanocrystalline and glassy coatings have been synthesized by electrodeposition method [33–38]. However, electrodeposition restricts coatings on large engineering components due to bath size limitation.

This study reports the large scale synthesis of Al based glassy coating by cold spraying. Cold spraying is suitable for synthesizing glassy metallic coating because of the low temperatures involved that retains the original phase structure. Since the cold spray is a solid-state process, grain growth and phase transformations are not expected. Moreover, unwanted effect such as oxidation is also avoided in the process. The bonding occurs due to plastic deformation caused by impact leading to consolidation of the powder particles onto the substrate [39]. Cold spraying can be performed on large size and shape of the substrate in the service environment. Cold sprayed Al-BMG coatings could be an alternative for the protection of the aircraft skin due to the inherent corrosion resistance of metallic glasses. These coatings can also be applied for the corrosion protection of ships and other components in the marine environment.

In this study, we have synthesized cold sprayed aluminum based glassy coatings on 6061-Al substrate. The coating, synthesized from amorphous Al-based powder, is characterized to understand its structural identity in terms of glassy behavior and microstructure. The coating is also studied to understand its wear and corrosion resistant properties.

2. Materials and methods

2.1. Powder and coating synthesis

A glassy powder with composition of $Al_{90.05}Y_{4.4}Ni_{4.3}Co_{0.9}Sc_{0.35}$ (at.%) was synthesized using high pressure gas atomization route [40]. Pure elements were first melted in a graphite crucible under argon atmosphere. Subsequently, the melt was poured into an argon gas stream for atomization. The details of the powder synthesis can be found elsewhere [40].

The coating was synthesized using cold spraying method at ASB Industries, Ohio. The powder was fed through a high-pressure hopper, mixed with the preheated (673 K) nitrogen in a mixing chamber inside the gun, and was deposited at a very high pressure (3.8 MPa) on to the 6061-Al substrate. The gas pressure and the temperature were monitored by diagnostic ports inside the gun. An X–Y manipulator and a lathe were used to scan the spray beam over the substrate surface. Substrate temperature was maintained ~323 K.

2.2. Powder and Coating Characterization

The structural characterization of powder and coating was carried out using X-ray diffraction (XRD) and differential scanning calorimetry (DSC). XRD patterns were obtained using Cu K_α ($\lambda = 1.542A°$) radiation in a Siemens D5000 X-ray diffractometer operating at 40 kV and 40 mA. A scan rate of 2°/min and a step size of 0.2° were used

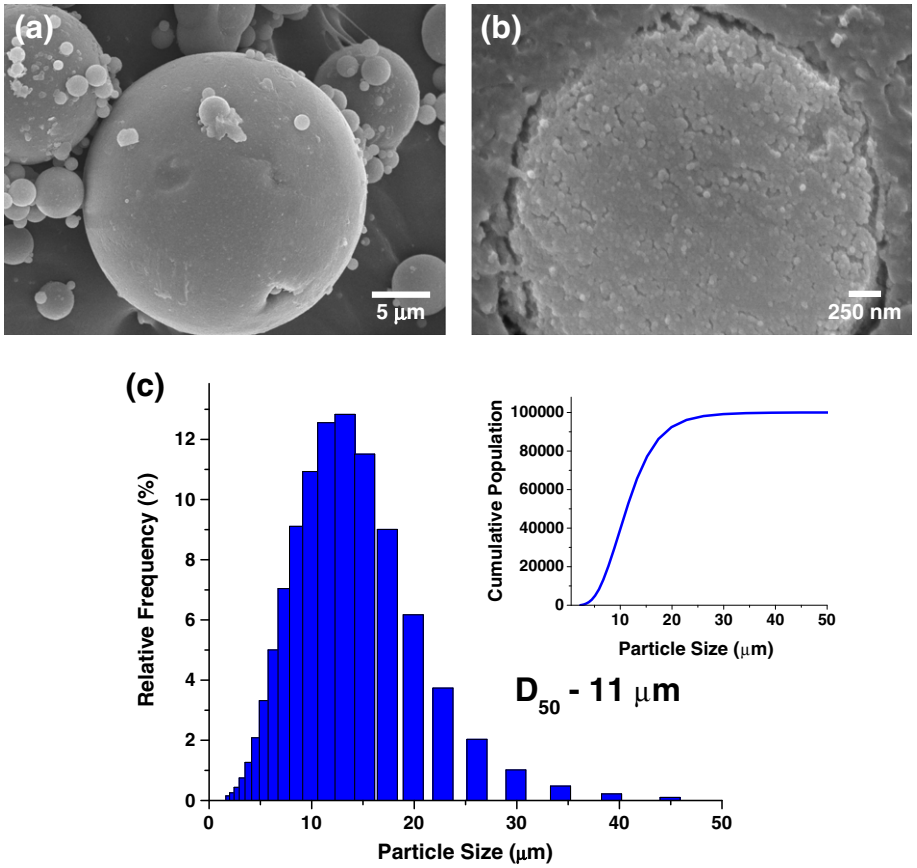

Fig. 1. SEM micrograph of (a) Al-BMG powder revealing the size distribution and (b) mounted and etched Al-BMG powder particle showing the agglomeration of nano-particle in it; (c) particle size distribution of the Al-BMG powder.

to obtain XRD profiles. DSC was carried out using DSC 2910 (Du Pont Instruments) at a heating rate of 10 K/min. Microstructural characterization of the powder and coating were carried out using JEOL JSM-633OF field emission scanning electron microscope, operating at 15 kV. The samples for microstructural observation were prepared by mounting powders and coated substrates in epoxy resin followed by conventional metallographical polishing procedure. Grinding was done using SiC particle embedded grit papers followed by polishing using alumina particle suspension. Keller's reagent was used as etchant for observing grain/splat structures. Philips/FEI Tecnai F30 high resolution transmission electron microscope (HRTEM) operating at an accelerating voltage of 300 kV was used to observe the coating structure. The TEM sample was prepared by gentle grinding of the coating surface using a minimal force. The coating particles were collected and ultrasonicated in ethanol for 5 min. These fine particles were placed on the grid in TEM sample holder and subjected to TEM investigation. The particles are thin enough to reveal the microstructure as seen in Fig. 4. Energy dispersive spectroscopy maps were obtained using JEOL JSM 5910LV SEM. Particle size analysis was done using laser diffraction and verified from SEM images.

2.3. Hardness Measurement

Microhardness of the coating and the substrate was evaluated using indentation techniques. Microhardness tester (Shanghai Taiming Optical Instrument Co. Ltd., model HXD-1000 TMC, Shanghai) with a Vickers probe was used for hardness measurement with an application of 200 g load for 15 s of dwell time. A minimum of 12 indents were made for each sample. Hardness at nano-scale was obtained using Hysitron Triboindenter (Hysitron Inc., Minneapolis, MN, USA) with 100 nm Berkovich pyramidal probe. The nanoindentation tests were carried out in quasi-static indentation mode with a peak load of 1000 μN, loading/unloading rate of 100 μN/s and dwell of 3 s at peak load. Nano-hardness of the as-received Al-BMG powder particle, in mounted and polished condition, was also measured using nanoindentation with the probe and load cycles similar to the coating. A minimum of 25 nanoindentation measurements were performed for the powder and coating samples. Powder hardness data was used to compute the plastic strain in the cold sprayed splat.

2.4. Wear Studies

Tribological behavior of the cold sprayed Al-BMG coating and 6061-Al substrate was studied using ball-on disk tribometer (Nanovea, CA). A 3 mm diameter aluminum oxide ball was used as the wear probe. The wear test was carried out on a 6 mm diameter circular track with a speed of 200 rpm. The tests were carried out for 5, 30 and 60 min. The profile of the wear track was obtained through optical profilometer PS50 (Nanovea, Irvine, CA) and the images were processed through SPIP version 5.1 (Image Metrology, Denmark). Volume of the wear tracks were calculated from the processed depth profiles. Coefficient of friction was also recorded during the wear tests.

2.5. Electrochemical Testing and Contact Angle Measurement

The potentiodynamic polarization tests were performed on coating and substrate, in accordance with ASTM: G 102-89 employing a GAMRY® potentiostat (G-750) at ambient conditions. A typical three electrode (working, counter and reference) corrosion cell interphased with a potentiostat was employed, with a scan rate of 1 mV/s over a potential range of −2.0 to 2.0 V_{SCE}. The exposed area of the working electrode to the electrolyte was 0.28 cm^2. Two different concentrations of NaCl (0.01 and 0.1 N) electrolyte were used by mixing the reagent grade chemical with distilled water. Prior to each electrochemical and contact angle measurement, samples were ultrasonically cleaned in 99.9% acetone for 5 min. Contact angles for coating and substrate were measured using a Kyowa contact angle meter (model DM-CE1) by adopting a sessile drop method with distilled water under ambient conditions. Five tests with an average spacing of ~0.5 mm between each drop were conducted.

3. Results and discussion

3.1. Powder and coating morphology

The gas atomized $Al_{90.05}Y_{4.4}Ni_{4.3}Co_{0.9}Sc_{0.35}$ powder was spherical in shape (Fig. 1a). SEM image of powders reveals smooth surface (Fig. 1a). The polished and etched powder particle revealed nanosize particles (10–20 nm), which agglomerated to form larger particles during atomization (Fig. 1b). The particle size analysis (Fig. 1c) furnishes a wide distribution with diameter ranging between 2.5 to 45 μm (D_{50} = 11 μm). The DSC plot shows two exothermic events occurring at 330 and ~350 °C in the powder (Fig. 2a). This is quite usual for multicomponent metallic glasses, which form several phases during their crystallization. These peaks indicate onset of crystallization, and thus the presence of glassy/amorphous phase in the powder.

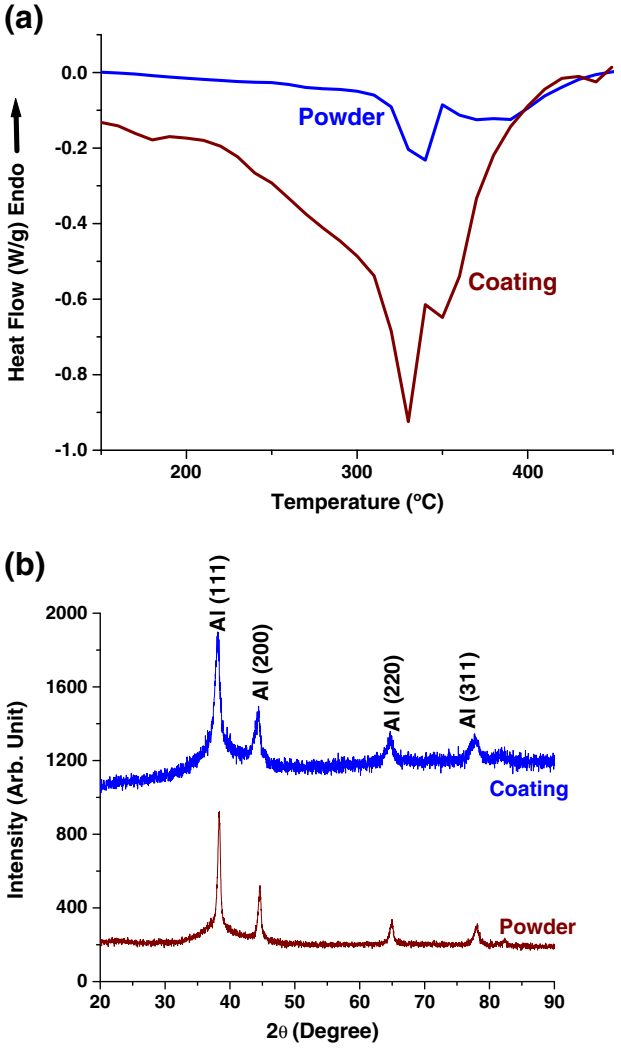

Fig. 2. (a) DSC plot of the Al-BMG powder and cold-sprayed coating revealing twin crystallization peaks; (b) XRD pattern of Al-BMG powder and cold-sprayed coating showing amorphous hump and few broad Al-FCC peaks.

The XRD pattern shows presence of a hump in the region of $2\theta = 30–50°$ (Fig. 2b), which also indicates the amorphous nature of the powder. However, the presence of broad Al-FCC peaks in the pattern confirms that the crystallization could not be avoided fully during gas atomization [41].

Fig. 3 shows the morphology and physical nature of the polished and etched cold sprayed coating synthesized using Al-BMG powders on 6061-Al substrate. The coating reveals a very dense (98%) structure and uniform thickness of ~250 μm (Fig. 3a). The elongated splats with trapped round powder particles in the coating are observed in Fig. 3b. The flattening and elongation of spherical glassy aluminum particles is attributed to the deformation caused by high pressure propelling and their collision against substrate surface during cold spraying. Papyrin et al. [39] have devised the empirical relationship for measuring the plastic strain (ε_p) in the individual particles from the deformed shape of cold spray deposited single particles as a function of materials properties. The relationship is as following:

$$\varepsilon_p = e\left(-1.4\frac{H_p}{\rho_p J_p^z}\right) \quad (1)$$

where, ε_p is the strain in the particle, H_p, ρ_p and ν_p are the hardness (in MPa), density and velocity of the powder particle. The velocity of the Al particles is found to be 500 m/s in similar conditions of cold spraying [42]. The hardness of the Al-BMG powder was measured to be 3.1 ± 0.5 GPa. The density of the powder is calculated to be 3.08 g/cm^3. Thus, using Eq. (1) the strain in the cold sprayed splats is approximated as 0.57. This strain indicates a significant amount of plastic deformation introduced during cold spraying, which is very impressive considering the glassy and usually brittle nature of the starting powder. The deformability in the glassy powder could be due to the crystalline part in the structure. The high magnification micrograph at interface of the Al-BMG coating with 6061-Al substrate shows a very strong bonding and no sign of delamination or cracking (Fig. 3c). The substrate shows a thin deformed interface with an excellent interlocking. The nano-size features of the starting powder (Fig. 1b) are retained in the coating in Fig. 3c.

The DSC plot for the coating also reveals twin crystallization peaks (Fig. 2a) at 330 and 340 °C. Presence of crystallization peaks in the coating indicates that glassy structure of the powder is carried forward after cold spraying. High amount of plastic deformation introduced during cold spraying is the source of extra enthalpy (energy flow) available in the splat structure of the coating. XRD pattern also reveals a prominent hump at ~30–50° with a few broad Al-FCC peaks, denoting presence of amorphous phase in the coating (Fig. 2b). A closer observation reveals the amorphous hump to be more prominent and Al peaks more broad in the coating as compared to the powder. This is the result of extensive low temperature deformation in Al-BMG powder structure during cold spraying, which further disturbs any atomic arrangement in the structure.

HR-TEM micrographs of the coating corroborate the inferences from DSC and XRD on the glassy structure of the coating. Fig. 4a does not show presence of any prominent lattice structure, characteristic of FCC aluminum. On the contrary, it reveals mostly amorphous structure with a few nanocrystals embedded in it. Fig. 4b reveals the traces of heavy deformation in the splat structure introduced during cold spraying of the Al-BMG powder. This heavy deformation could also break the crystalline phase in the powder into nanocrystals. Though the powder was mixed with preheated nitrogen at 673 K, but the short residence time (millisecond) of powder with the heated gas and the consequent heavy deformation helps in retaining the

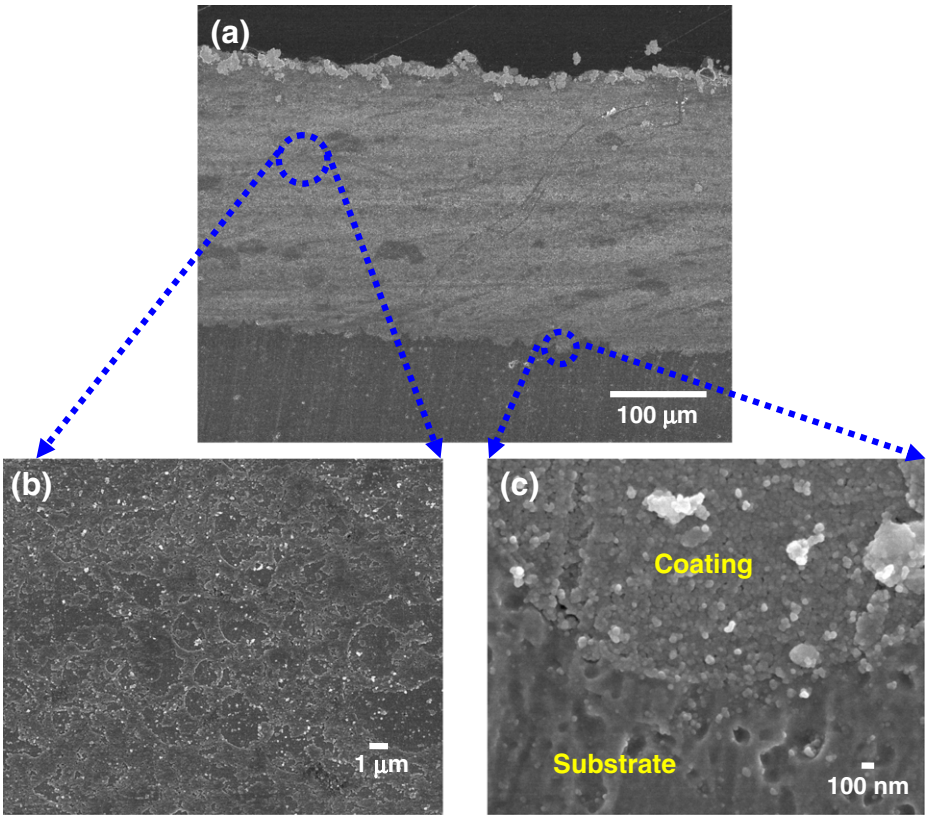

Fig. 3. SEM micrographs of cold sprayed Al-BMG coating cross section revealing the (a) uniform thickness; (b) cold sprayed splat structure and (c) good bonding with Al-6061 substrate.

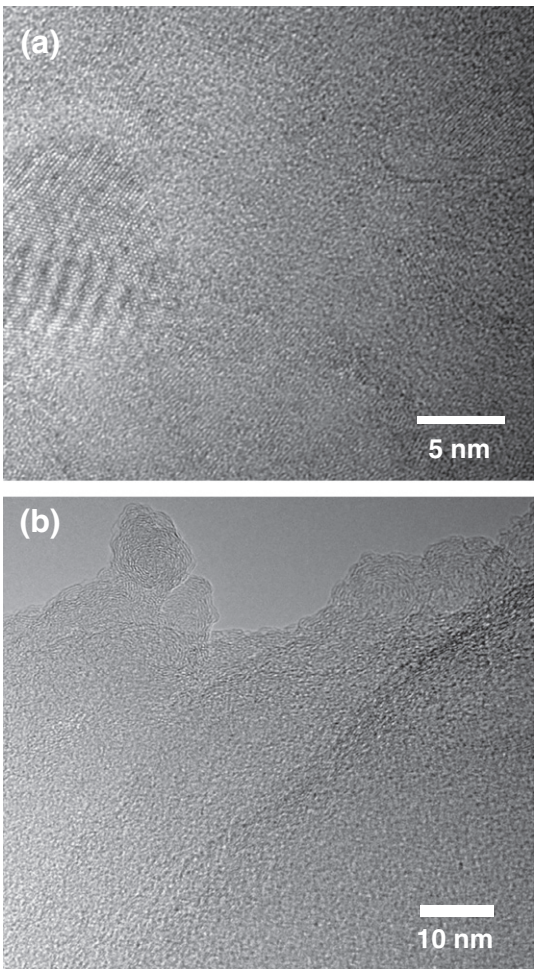

Fig. 4. HRTEM images of cold sprayed Al-BMG coating revealing the (a) mostly amorphous stricture with few nanocrystals embedded and (b) severe deformation caused by cold spraying.

amorphous structure in coating, as observed in XRD and HRTEM results.

3.2. Hardness of the Coating and Powder

The microhardness of Al-BMG coating and 6061-Al substrate is 3.36 ± 0.11 GPa and 1.09 ± 0.02 GPa, respectively. The nano-hardness of Al-BMG powder was measured as 3 ± 0.02 GPa, which increased to 5.01 ± 0.41 for cold sprayed coating. This increase in hardness of the glassy powder to amorphous coating is attributed to the high strain (0.57) introduced during the cold spraying, which causes strain hardening. The difference in the hardness values of the coating at micro and nano-scale length is attributed to the splat structure of the coating, which is heterogeneous and very sensitive to the scale of the measurement.

3.3. Tribological Behavior of the Coating

Fig. 5a presents the wear volume vs. traverse time plot for the substrate and coating. The depth profile of the wear track across the width is presented in Fig. 5b. Al-BMG coating shows a maximum wear depth of 30 μm after 60 min whereas 6061-Al substrate shows a significantly higher wear depth of 135 μm. The corresponding 3D wear profiles obtained from optical profilometry, are shown in Fig. 5a which provide a true sense of the wear volume of coating and substrate. A significant 600% lower wear volume loss is noted in the cold sprayed Al-BMG coating as compared to the uncoated 6061-Al substrate. Fig. 5c shows the coefficient of friction (COF) of the coating and the substrate during the ball-on-disk wear. The COF for coating stabilizes after 8 min of wear and shows a steady value of 0.45, whereas COF for the substrate shows a dual regime and a higher value (0.6–0.75). The wear mechanism could be understood by observing the worn surfaces.

Fig. 6a–d shows the wear tracks on 6061-Al substrate and Al-BMG coating at different magnifications, revealing wear morphologies. Fig. 6a and c present low magnification SEM images of the portion of wear tracks on 6061-Al substrate and Al-BMG coating, respectively. The 6061 Al substrate shows severe damage and roughness in the wear track, whereas the worn surface of coating is much smoother with less damage. The wear of 6061-Al substrate is accompanied by plowing, which creates deep craters with coarse stretch signs denoting material removal (Fig. 6b). This is a common feature of the wear in softer metals. On the contrary, the wear track on Al-BMG coating is much smoother and free of plowing. Smoother surface in wear track of BMG (Fig. 6d) is the sign of abrasion dominated wear, which is a common characteristic of hard materials like bulk metallic glasses [11,12,16]. No cracks were observed on the coating surface despite its high hardness. The wear mechanism can also be correlated with COF. Initially, the wear in 6061-Al substrate is dominated by plowing. More lateral force is required for removal of material in plowing. The craters created by plowing produce a rougher surface, which leads to a higher COF as compared with the coating. At a later stage (30 min), fine particles generated as wear debris offer some lubrication and the COF is comparatively reduced. In the case of cold sprayed Al-BMG coating, COF shows high value and more noise initially due to the higher hardness and slippage of the glassy surface. Once an impression of wear track is created (~8 min), the wear is mainly dominated by light abrasion which is shown as smooth scar. Thus, the surface remains comparatively smooth with a lower COF than 6061-Al substrate.

3.4. Corrosion behavior of the coating

Fig. 7 shows typical potentiodynamic polarization curves for the substrate and coated sample in 0.01 N and 0.1 N NaCl electrolytes. A Tafel fit was employed to analyze the polarization curves, and corrosion rates were obtained by extrapolating the Tafel slopes. The substrate exhibited higher passive current (9.8–28.7 μA) as compared with the coating (2.0–6.3 μA), as shown in Table 1. Coated samples showed reduction in cathodic and anodic currents, when compared with currents corresponding to the substrate. The corrosion rate (mpy) of the substrate is 5 times greater than that of the coating for both 0.01 and 0.1 N NaCl electrolytes, indicating excellent corrosion resistance of the cold sprayed Al-BMG coating. Additionally, the coating displayed multiple regions of passivity in 0.1 N NaCl electrolyte, which may be due to the initial instability of the passive oxide film, followed by new oxide layer formation.

The high corrosion resistance of the coating can be attributed to two main features. Firstly, amorphous nature of the coating leads to chemical homogeneity making it difficult for the formation of localized galvanic cells and the onset of corrosion. Furthermore, the presence of nanocrystals, as evidenced in HRTEM micrograph, leads to improvement in the corrosion resistance. Accelerated passive film formation in nanocrystal containing amorphous structure has been reported, due to the enhanced diffusion of passive elements [6,7,18]. The accelerated nature of passivation is also corroborated by the potentiodynamic curve in Fig. 7b. Fig. 8a and b show SEM images of coating surface before and after corrosion. Elemental distribution maps for Al and O corresponding to Al_2O_3 film formation on Al-BMG

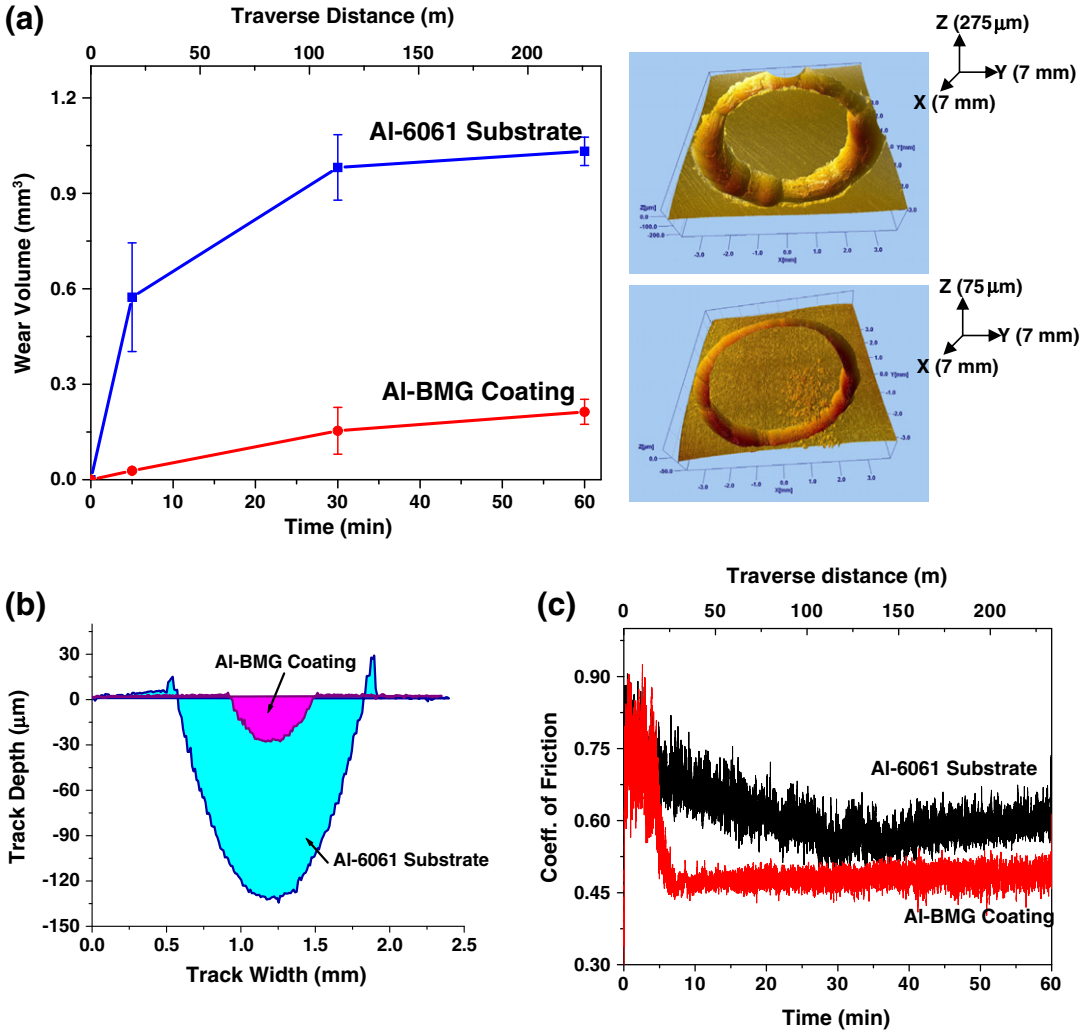

Fig. 5. (a) Wear Volume vs. time plot with respective SPM images for tracks at 60 min; (b) profile of the track across width after 60 min; (c) coefficient of friction vs. time plot for Al-BMG coating and Al-6061 substrate.

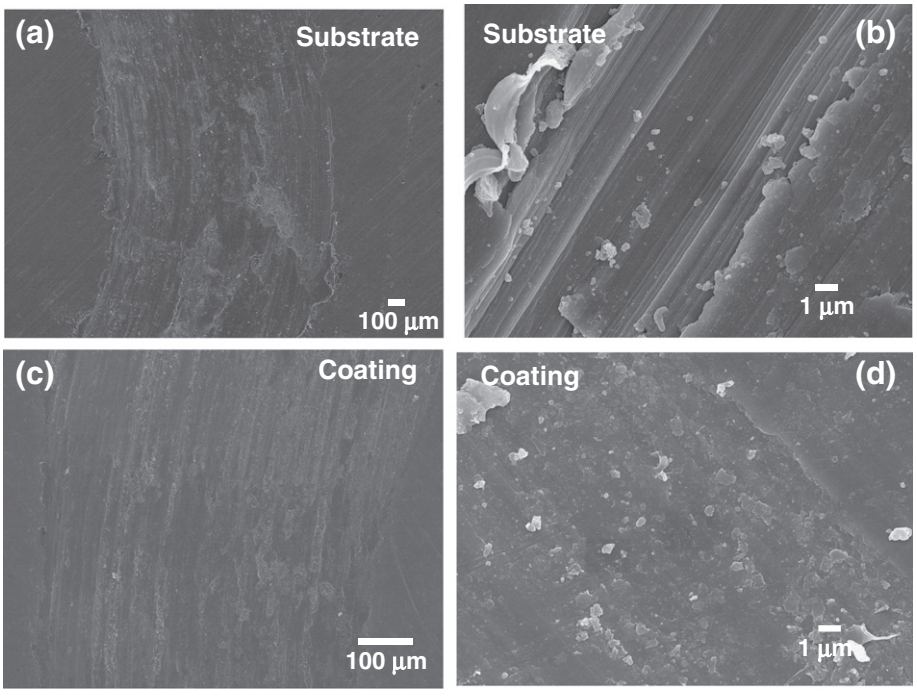

Fig. 6. SEM micrographs of wear track on (a–b) Al-6061 substrate revealing plowing of material; (c–d) Al-BMG coating showing the smoother surface and less wear.

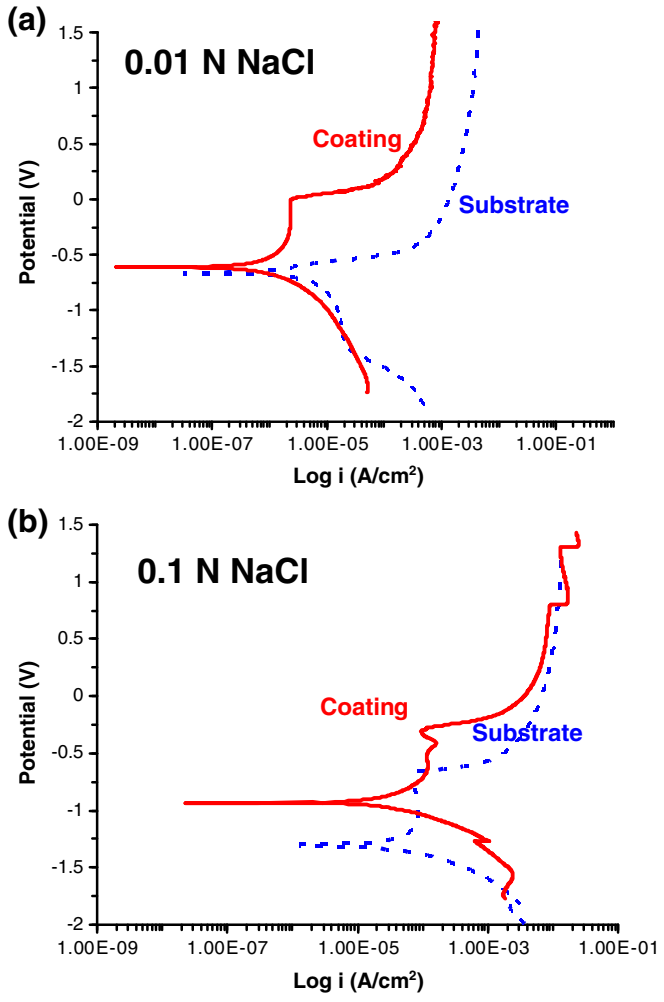

Fig. 7. Potentiodynamic polarization curves for Al-6061 substrate and Al-BMG coating in (a) 0.01 and (b) 0.1 N NaCl electrolyte.

coating before and after corrosion in 0.1 N NaCl are also shown in Fig. 8. The surface after corrosion shows uniform and high oxygen content (Fig. 8d), which is minimal before corrosion (Fig. 8c). This indicates the formation of a passive oxide layer during corrosion. Conventionally, FCC Al with nanocrystallites, shows a higher probability of pit formation. However, no severe pitting is observed in SEM micrograph (Fig. 8b) of the coating after corrosion. The lack of severe pitting is attributed to the amorphous matrix, which is rich in substitutional elements and surrounds the nanocrystals. It requires a higher potential than that required for pure Al to maintain a stable pit growth condition [5]. Thus, severe pitting is not observed in cold sprayed Al-BMG coating.

Contact angle on 6061-Al substrate revealed hydrophilic (88.6 ± 2.1°) behavior with polar solvent (water). The coating displayed hydrophobic nature with an increased contact angle (118.3 ± 0.9°). The higher contact angle for the coating can also be correlated to a higher corrosion resistance as contact area and surface energy is minimized.

Table 1
Corrosion behavior of Al-BMG coating and Al-6061 substrate at different concentrate of NaCl bath.

Sample/bath	Ecorr, V	Icorr, μA	Corr Rate, mpy
Coating/0.01 NaCl	−0.705	1.960	3.012
Coating/0.1 NaCl	−0.869	6.260	9.593
Substrate/0.01 NaCl	−0.661	9.870	15.14
Substrate/0.1 NaCl	−1.310	28.7	44.0

4. Conclusions

Cold spraying of amorphous Al based powder is established as a suitable technique for large scale synthesis of Al-BMG coating. The coating is highly dense, uniform, shows good adhesion and retains the glassy nature. The coating exhibits high hardness due to its glassy nature leading to 600% higher wear resistance than 6061-Al substrate. The corrosion resistance of the coating is 5 times greater than the 6061-Al substrate in different NaCl concentrations. The improved corrosion resistance results from the chemical homogeneity of the amorphous structure with embedded nanocrystals. Cold sprayed Al-based amorphous coating shows great promise in protecting aluminum surface from corrosion and wear.

Acknowledgment

The authors at Florida International University acknowledge the research facilities at Advanced Materials Engineering and Research Institute (AMERI) for providing various characterization facilities.

References

[1] A. Inoue, Prog. Mater. Sci. 43 (1998) 365.
[2] A. Inoue, Acta Mater. 48 (2000) 279.
[3] A.K. Gangopadhaya, T.K. Croat, K.F. Kelton, Acta Mater. 48 (2000) 4035.
[4] F. Schurack, J. Eckert, L. Schultz, Acta Mater. 49 (2001) 1351.
[5] J.E. Sweitzer, G.J. Shiflet, J.R. Scully, Electrochim. Acta 48 (2003) 1223.
[6] W. Xueqing, M. Mo, T. Chaogui, W. Xiufeng, L. Jianguo, J. Rare Earths 25 (2007) 381.
[7] J.G. Lin, W.W. Wang, X.Q. Wu, J.H. Lei, S. Yin, J. Alloys Compd. 478 (2009) 763.
[8] A. Roy, A.K. Mandhyan, K.L. Sahoo, J. Banhart, I. Chattoraj, Mater. Corros. 60 (2009) 431.
[9] K.G. Prashanth, S. Scudino, B.S. Murty, J. Eckert, J. Alloys Compd. 477 (2009) 171.
[10] J. Mu, H. Fy, Z. Zhu, A. Wang, H. Li, Z. Hu, H. Zhang, Adv. Eng. Mater. 11 (2009) 530.
[11] M.Z. Ma, R.P. Liu, Y. Xiao, D.C. Lou, L. Liu, Q. Wang, W.K. Wang, Mater. Sci. Eng., A 386 (2004) 326.
[12] N. Togashi, M. Ishida, N. Nishiyama, A. Inoue, Rev. Adv. Mater. Sci. 18 (2008) 93.
[13] Z. Parlar, M. Bakkal, A.J. Shih, Intermetallics 16 (2008) 34.
[14] D. Huang, R. Li, L. HUang, V. Ji, T. Zhang, Intermetallics 19 (2011) 1385.
[15] Q. Chen, K.C. Chan, L. Liu, Phil. Mag. 91 (2011) 3705.
[16] D. Zenebe, S. Yi, S.S. Kim, J. Mater. Sci. 47 (2012) 1446.
[17] T. Gloriant, J. Non-CRyst. Solids 316 (2003) 96.
[18] X.F. Wang, X.Q. Wu, J.G. Lin, M. Ma, Mater. Lett. 61 (2007) 1715.
[19] M. Gogebakan, P.J. Warren, B. Cantor, Mater. Sci. Eng., A 226–228 (1997) 168.
[20] X. Bian, M. Sun, Mater. Lett. 57 (2003) 2460.
[21] J. Basu, S. Ranganathan, Intermetallics 12 (2004) 1045.
[22] H.W. Yang, W.P. Tong, X. Zhao, L. Zuo, J.Q. Wang, J. Alloys Compd. 473 (2009) 347.
[23] K. Song, X. Bian, X. Lu, J. Guo, G. Li, M. Xie, Mater. Sci. Eng., A 506 (2009) 87.
[24] B.J. Yang, J.H. Yao, J. Zhang, H.W. Yang, J.Q. Wang, E. Ma, Scripta Mater. 61 (2009) 423.
[25] H.J. Kim, K.M. Lim, B.G. Seong, C.G. Park, J. Mater. Sci. 36 (2001) 49.
[26] X. Wu, B. Xu, Y. Hong, Mater. Lett. 56 (2002) 838.
[27] D.J. Sordelet, M.F. Besser, Mater. Sci. Eng., A 375–377 (2004) 625.
[28] H. Choi, J. Kim, C. Lee, K.H. Lee, J. Mater. Sci. 40 (2005) 3873.
[29] A.P. Wang, Z.M. Wang, J. Zhang, J.Q. Wang, J. Alloys Compd. 440 (2007) 225.
[30] H. Cho, H. Choi, H. Jo, S. Lim, B. Kim, C. Lee, Mater. Sci. Eng., A 449–451 (2007) 118.
[31] A. Kobayashi, S. Yano, H. Kimura, A. Inoue, Mater. Sci. Eng. B 148 (2008) 110.
[32] X.Q. Liu, Y.G. Zheng, X.C. Chang, W.L. Hou, J.Q. Wang, Z. Tang, A. Burgess, J. Alloys Compd. 484 (2009) 300.
[33] J.C. Li, S.H. Nan, Q. Jiang, Surf. Coat. Technol. 106 (1998) 135.
[34] Z. El Abedin, P. Giridhar, P. Schwab, F. Endres, Electrochem. Commun. 12 (2010) 1084.
[35] J. Pan, W.T. Tsai, I.W. Sun, Electrochem. Solid-State Lett. 13 (2010) D69.
[36] Y. Ruan, C.A. Schuh, Acta Mater. 57 (2009) 3810.
[37] K. Chang, S.Y. Chen, C.H. Tseng, W.T. Tsai, Electrochemistry 77 (2009) 585.
[38] J.F. Zhang, C.W. Yan, F.H. Wang, Appl. Surf. Sci. 255 (2009) 4926.
[39] A. Papyrin, V. Cosarev, S. Klinkov, A. Alkhimov, V. Fomin, in: A. Papyrin (Ed.), Cold Spray Technology, Elsevier, Oxford, 2007, p. 33.
[40] D.J. Sordelet, E. Rozhkova, P. Huang, P.B. Wheelock, M.F. Besser, M.J. Kramer, J. Mater. Res. (2002) 186.
[41] S. Scudino, K.B. Surreddi, H.V. Nguyen, G. Liu, T. Gemming, M. Sakaliyska, J.S. Kim, J. Vierke, M. Wollgarten, J. Eckert, J. Mater. Res. 24 (2009) 2909.
[42] S.R. Bakshi, V. Singh, K. Balani, D. Graham McCartney, S. Seal, A. Agarwal, Surf. Coat. Technol. 202 (2008) 5162.

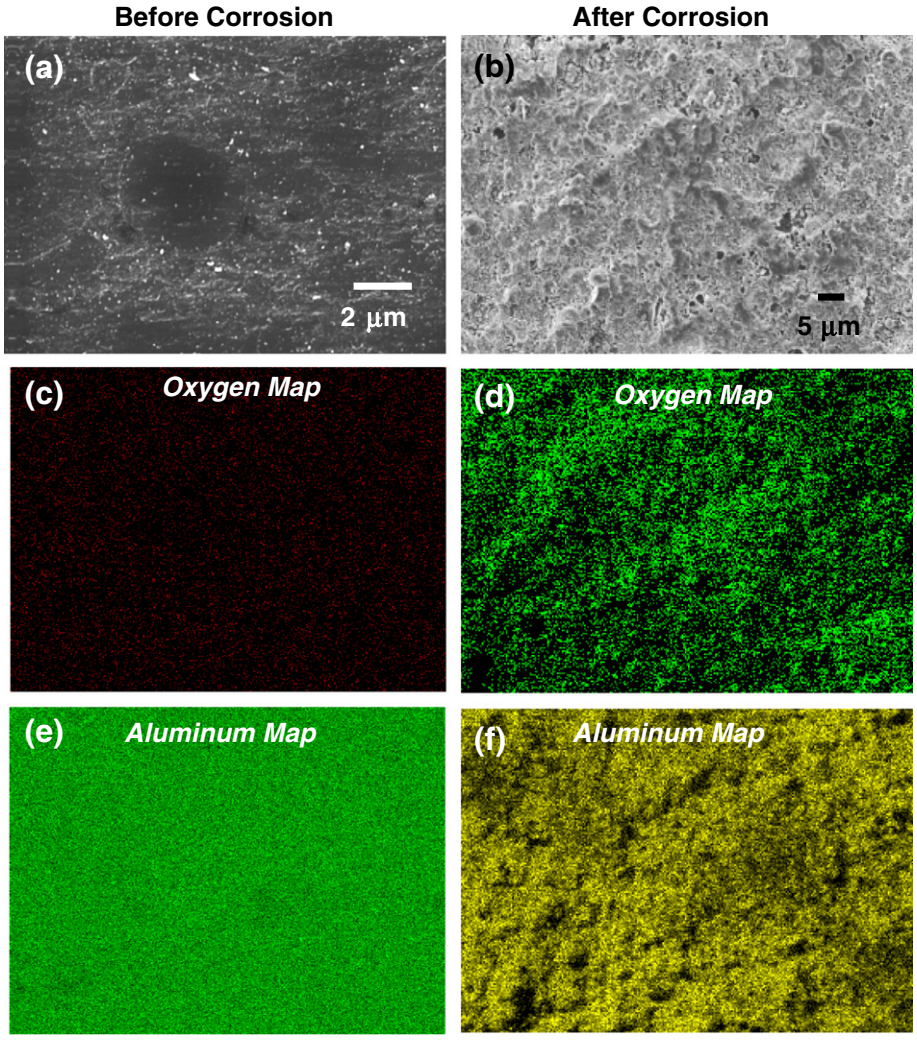

Fig. 8. SEM micrographs of Al-BMG coating surfaces (a) before and (b) after corrosion in 0.1 N NaCl bath. EDS analysis of the regions in SEM images reveals (c–d) elemental oxygen distribution and (e–f) elemental aluminum distribution.